

Finite-Size Effects of a Left-Handed Material Slab on the Image Quality

Long Chen,¹ Sailing He,^{1,2,*} and Linfang Shen¹

¹Centre for Optical and Electromagnetic Research, State Key Laboratory of Modern Optical Instrumentation, Joint Research Center of Photonics of the Royal Institute of Technology (Sweden) and Zhejiang University, Zhejiang University, Hangzhou, 310027, China

²Laboratory of Photonics and Microwave Engineering, Department of Microelectronics and Information Technology, Royal Institute of Technology, S-16440 Kista, Sweden

(Received 29 June 2003; published 12 March 2004)

The characteristics of an imaging system formed by a left-handed material (LHM) slab of finite length are studied, and the influence of the finite length of the slab on the image quality is analyzed. Unusual phenomena such as surface bright spots and negative energy stream at the image side are observed and explained as the cavity effects of surface plasmons excited by the evanescent components of the incident field. For a thin LHM slab, the cavity effects are found rather sensitive to the length of the slab; the bright spots on the bottom surface of the slab may stretch to the image plane and degrade the image quality.

DOI: 10.1103/PhysRevLett.92.107404

PACS numbers: 78.20.Ci, 42.30.Wb, 73.20.Mf

Recently, a new type of composite material [also called left-handed material (LHM)] that exhibits simultaneously negative effective permittivity and permeability over a certain frequency band has attracted great attention [1–4]. Theoretically an infinitely extended LHM slab can reconstruct the original object and achieve a perfect resolution under an ideal case (i.e., the so-called perfect lens) [3]. While the inherent material loss greatly suppresses the amplification of evanescent waves and makes the perfect image impossible [5], subwavelength imaging is still achievable for a thin LHM slab [6]. However, in a realistic imaging system the length of the LHM slab must also be finite, particularly for applications such as microdetectors and microimaging devices where the device size is required to be as small as possible. In this Letter, we study the effects of the finite size of the LHM slab to the imaging quality. A finite-difference time-domain (FDTD) method [7] is used in the numerical simulation.

The two-dimensional (2D) imaging system we consider here is a planar LHM slab (surrounded by vacuum) with a finite length of L and a thickness of d . The slab is located in the region of $(-L/2 < x < L/2, 0 < z < d)$, and a point source located at $(x = 0, z = -u)$ is used to generate the object for the imaging system [see the left panel of Fig. 1]. Here we consider only the E polarization where \mathbf{E} is directed in the y direction. For matched material parameters and $u < d$, the field is focused at $z = u$ inside the slab and $z = 2d - u$ outside the slab [3]. Here for simplicity we set $u = 0.5d$ in all our imaging simulations. To avoid the field singularity of the point source, the *object* plane is selected to be slightly (0.05λ) below the point source, and the *image* plane is shifted correspondingly. The computational domain is bounded by perfect-matched layers and a FDTD method of scattered-field and/or total-field version is adopted [7]. To avoid the divergence (occurred when the permittivity and permeability are negative) as the time marches in

the FDTD simulation, the following Drude's dispersion model [8] for the permittivity and permeability of the LHM slab is used:

$$\varepsilon(\omega) = \varepsilon_0 \left(1 - \frac{\omega_{pe}^2}{\omega^2} \right), \quad \mu(\omega) = \mu_0 \left(1 - \frac{\omega_{pm}^2}{\omega^2} \right). \quad (1)$$

The permittivity and permeability take negative values for frequencies below ω_{pe} and ω_{pm} , respectively. Here we assume $\omega_{pe} = \omega_{pm}$ and the material parameters are matched [i.e., $\varepsilon(\omega_0)/\varepsilon_0 = \mu(\omega_0)/\mu_0 = -1$, as assumed for a perfect lens] at frequency $\omega_0 = \omega_{pe}/\sqrt{2}$. To minimize the frequency extension, the time dependence of the point source is set as $\exp(i\omega_0 t)f(t)$, where $f(t)$ is a step function that reaches 1 smoothly in a time duration of $30T_0$ (here the period $T_0 = 2\pi/\omega_0$). The grid size of the discretization is 0.01λ . After enough time steps, the field evolution becomes stable, and the stable field is taken as the field at frequency ω_0 (the accuracy has been verified by taking the Fourier transform of the time sequence of the field to extract the field at frequency ω_0 , and thus the dispersion effect is negligible for our monochromatic incidence).

Unusual phenomena.—Interesting phenomena can be observed clearly from Fig. 1(a) for the distributions of the normalized field intensity and z component of the energy stream (S_z) on the image plane. Here we choose $L = 8\lambda$ and $d = 0.2\lambda$. Unlike the ideal imaging for an infinitely extended LHM slab, next to the central peak (the desired image) the image for a LHM slab of finite length has additional peaks with considerable magnitudes (even exceeding the magnitude of the central peak in some cases). More surprisingly, near the central peak the energy stream S_z has large negative values (reaching about -20% after normalization for this example). The negative S_z on the image plane seems counterintuitive since there is no scatterer below the slab and the normal energy stream there should simply

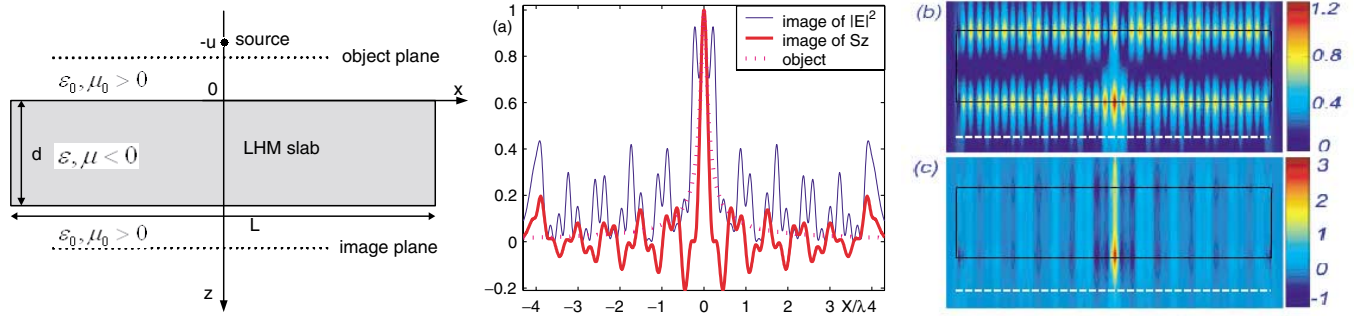


FIG. 1 (color online). Left panel: the geometry of the imaging system formed by a LHM slab of finite length. (a) Normalized distribution of field intensity (thin line) and the energy stream S_z (thick line) along the image plane for $L = 8\lambda$ and $d = 0.2\lambda$; here the normalized field intensity of the object is plotted (dotted line) for comparison. The corresponding 2D distribution of (b) $|E|^2$ and (c) S_z . Here the LHM slab and the image plane are marked with a rectangle and a dashed line, respectively.

flow downward (i.e., positive S_z) from the slab. The corresponding 2D distribution of the field intensity is shown in Fig. 1(b). Clearly one sees many bright spots (nearly equidistant) distributed along each surface of the LHM slab. Although the field decreases exponentially away from these surface spots, they still stretch to the image plane due to their large magnitudes and, consequently, damage the image. The two additional peaks in Fig. 1(a) on the image plane are the extension of the two brightest spots centered on the bottom surface of the slab [see Fig. 1(b)]. We have increased d (up to 3λ) and varied L (from 1.5λ to 9λ), and these unusual phenomena are still observed.

Cavity effects.— In the imaging system of infinitely extended LHM slab with matched material parameters, incident evanescent wave experiences amplification inside the slab and thus has strong intensity around the exit (i.e., bottom) interface of the slab (see, e.g., [3]). This wave can be conceived as a localized field around this single interface and is exponentially decreasing both into the slab and below the slab. Therefore, the simple term “surface plasmon” (commonly used for a surface-localized wave in metal-related electromagnetism) is “borrowed” to describe this evanescent wave with large field amplitude near the interface. For a point source located above the slab, the field intensity on the upper or bottom surface has a simple profile with only one central peak. Neither the additional surface bright spots nor negative energy stream can be observed for such an infinitely extended LHM slab. However, when the slab has a finite length, each excited surface plasmon can be roughly conceived as traveling along the bottom surface and encountering a side-end (i.e., the left or right boundary) of the slab. The main part of the energy should be reflected at this side-end since the surface plasmon exists only at the slab interface (however, a propagating wave goes through this side-end since the material parameters are matched). The remaining part runs across the corner or couples to radiation. The original and the multiply reflected waves are superimposed to form a standing wave profile. Therefore, the side-ends act as reflecting

walls and thus form a one-dimensional cavity for the surface plasmons. This lateral cavity effect leads to the distribution of nearly equidistant bright spots (due to the nodal structure of the standing wave) along the exit interface of the LHM slab. Meanwhile, the energy stream S_z along the surface of the slab has an oscillating behavior (with a period similar to that of the surface bright spots) and takes negative values at some positions, as shown in Fig. 1(c). Because of the continuity of the normal stream S_z on the bottom surface, these negative streams extend to the image plane and cause negative values at the image side. Note that the meaning of surface plasmon used here differs from that of “surface polariton” (or “slab plasmon polariton”), which usually refers to the coupled surface waves on both interfaces, i.e., symmetrical or antisymmetrical eigenmodes of the slab. Such eigenmodes do not exist for a LHM slab with an infinite length and matched material parameters (see, e.g., [6,9]).

Here we show that these bright spots and negative energy streams result from the resonance of surface plasmons, which are excited only by the evanescent components of the incident wave. Filters for the spatial spectrum are employed to extract the propagating or evanescent components of the incident field. The incident fields are first Fourier transformed with respect to x . A window function is applied to these spectra and the modified spectra are then transformed back to the physical space through the inverse Fourier transform. Therefore, a low-pass window function with the upper truncation $k_x = k_0$ extracts the propagating components of the incident field, while a high-pass window function with the lower truncation $k_x = k_0$ extracts the evanescent components. For graphic clarity we consider here a slab with $L = 2\lambda$ and $d = 2u = 0.2\lambda$. Note that the length of this slab is not too short since k_x has a large value [corresponding to a small period of oscillation in the x direction; for example, there are about nine nodes over the slab length of 2λ in Fig. 2(a) below]. The 2D field intensity distributions contributed by the full spectrum, the propagating parts, and the evanescent parts of the incident field are shown in Figs. 2(a)–2(c), respectively. The field intensity contributed by the

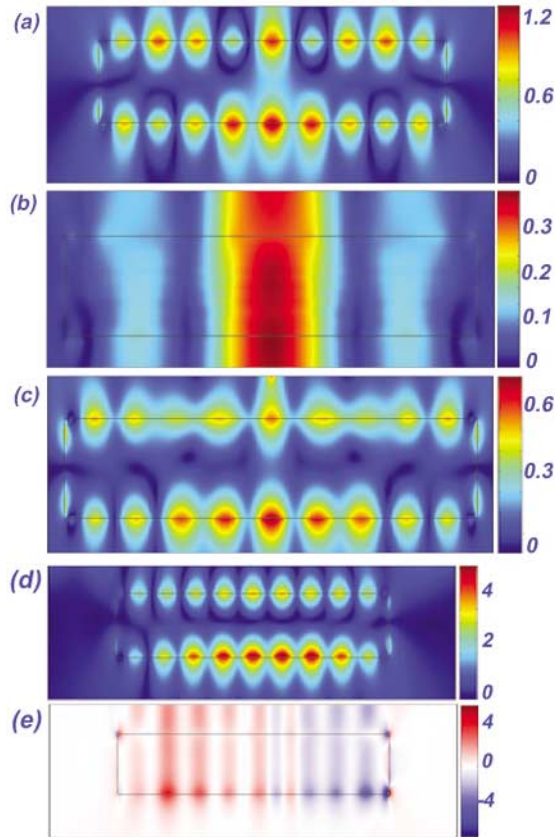


FIG. 2 (color online). (a)–(c) The 2D distribution of the field intensity after applying a filter to the spatial spectrum of the incident field generated by a point source: (a) with the full spectrum; (b) with only the propagating parts; and (c) with only the evanescent parts of the spatial spectrum. (d),(e) The 2D distributions of the field intensity and S_z , respectively, when the resonance is excited by a single evanescent wave with $k_x = 2k_0$. Here $L = 2\lambda$ and $d = 2u = 0.2\lambda$.

propagating components [Fig. 2(b)] is rather simple, with no reflection at the upper and bottom interface (as expected). The small neighboring peaks are due to the limited wave numbers for the propagating parts ($k_x < k_0$). However, the field intensity contributed by the evanescent components [Fig. 2(c)] has a similar distribution of surface bright spots (only a slight difference in their relative magnitudes) as compared with Fig. 2(a) for the case of full spectrum. We have also compared the energy streams along the image plane for these cases. The stream S_z has a simple profile and is non-negative everywhere when only the propagating components are included, while oscillating behavior and negative values are observed when the evanescent components are included.

We can numerically simulate the resonant behavior of a single evanescent wave for our imaging system. The 2D distributions of the field intensity and energy stream for the case of $L = 2\lambda$, $d = 0.2\lambda$, and $k_x = 2k_0$ are shown in Figs. 2(d) and 2(e), respectively. Equidistant bright spots along the surface with a period of $\pi/k_x = 0.25\lambda$ are clearly seen in Fig. 2(d), while in Fig. 2(e) the energy stream S_z exhibits an oscillating

property with alternating positive and negative values along the x direction. We have also carried out simulation for other values of L when the thickness d is fixed. Our numerical results show that as L increases the resonance strength (defined as the maximal field intensity $|E|_{\max}^2$ along the bottom surface) oscillates with multiple peaks, which resembles the resonant behavior of a simple one-dimensional resonator.

In addition to the lateral resonance caused by the reflection at the side-ends as analyzed above, the bright spots along the upper surface [see, e.g., Fig. 2(d)] suggest a coupling mechanism between the upper and bottom surfaces through the side-ends of the slab, and can be explained here by a dynamic procedure. For a LHM slab of infinite length with matched material parameters, the amplification of a single evanescent wave should produce strong field intensity only around the bottom surface. However, for a LHM slab of finite length, along the bottom surface the amplified evanescent wave diffracts near the side-ends (the corners) and couples some part of energy back into the slab. Like an additional evanescent wave incident from the other side of the slab, the diffracted wave also experiences an amplification inside the slab and leads to an enhanced field along the upper surface. Similar diffractions happen recursively around both surfaces until a stable field distribution with bright spots on both surfaces is established. This introduces a cavity effect along the z direction and thus the whole slab of finite length actually behaves like a two-dimensional cavity. The field evolution in our FDTD simulation verifies this dynamic procedure, and under some cases (e.g., $L = 2.2\lambda$, $k_x = 2.8k_0$) the field strength along the upper interface becomes much stronger than that along the bottom interface.

Here we give some numerical analysis for the two-dimensional cavity effects. Figures 3(a) and 3(b) show the dependences of the resonant strength on the wave vector k_x for different L (with the thickness $d = 0.2\lambda$) and different d (with the length $L = 2.0\lambda$), respectively.

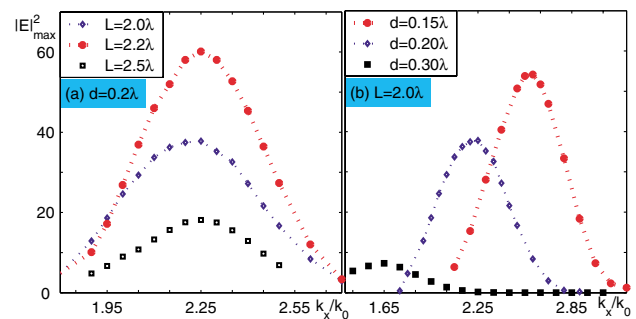


FIG. 3 (color online). Dependence of the resonant strength on k_x (a) when the length $L = 2.0\lambda$ (diamonds), 2.2λ (dots), and 2.5λ (squares) and the thickness d of the slab is fixed to 0.2λ , and (b) when the thickness $d = 0.15\lambda$ (filled circles), 0.2λ (diamonds), and 0.3λ (squares) and the length L of the slab is fixed to 2.0λ .

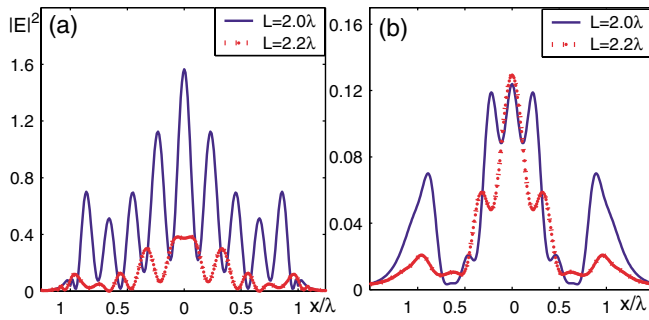


FIG. 4 (color online). Field intensity profiles (a) along the bottom surface of the LHM slab, and (b) along the image plane, when the incident field is generated by a point source. Here $d = 2u = 0.2\lambda$.

For a fair comparison between different k_x , we choose the source position $u = d$ to balance the amplification of evanescent waves inside the slab and their decay above the slab. The resonant strength has a selective effect with respect to k_x and has multiple resonant peaks [for graphic clarity we show in Fig. 3(a) only the strongest peak at $k_x \approx 2.25k_0$]. From Fig. 3(a) one sees that the peak positions of the resonant strength for different L do not change much (however, their peak values differ significantly, as mentioned before). This is because the resonant k_x (corresponding to the strongest resonance along the slab surfaces) depends strongly on the thickness d (due to the coupling between the two slab surfaces). The length L mainly influences the magnitude of the resonance. As shown in Fig. 3(b) for $L = 2.0\lambda$, the peak positions are at $k_x \approx 2.6k_0$, $2.25k_0$, and $1.65k_0$ when $d = 0.15\lambda$ (filled circles), 0.2λ (diamonds), and 0.3λ (squares), respectively. The corresponding peak values decrease by about one order when d increases from 0.15λ to 0.3λ (as the coupling between the two slab surfaces decreases).

An incident field generated by a point source contains many evanescent waves. Since the resonant strength of each evanescent component is sensitive to the length L , the image profile of a point source depends greatly on L . A simple comparison for the field intensity profiles along the bottom surface and the corresponding images are shown in Figs. 4(a) and 4(b) for two slightly different values of L (i.e., $L = 2\lambda$ and 2.2λ), respectively. Here the thickness is still kept as $d = 0.2\lambda$. Much brighter surface spots exist for $L = 2\lambda$, and along the image plane the two unwanted large peaks around $x = \pm 0.23\lambda$ are the extension of the two distinct surface spots centered on the bottom surface of the slab. Contrarily, the case of $L = 2.2\lambda$ gives a flattened central spot and weaker field in the neighboring region, and thus the image quality is better as compared with that for $L = 2\lambda$. As we increase L further, the field intensity profiles are found to exhibit a quasiperiodic behavior. For $L = 2.4\lambda$, the image quality becomes poor again with two unwanted peaks greatly exceeding the central peak by more than 130%. The additional surface spots still exist and degrade the image quality for L up to 9λ . As L increases, the image quality

varies between the worst image quality (at, e.g., $L = 2.4\lambda$) and the best image quality (at, e.g., $L = 8.2\lambda$) with the full width at half maximum (FWHM) of about 0.24λ (the FWHM of the object is about 0.22λ), while the distance between these resonant peaks decreases quickly (e.g., from about 0.23λ to 0.11λ when we increase L from 2λ to 9λ). For a sufficiently long slab, the lateral nodal structures are expected to partially cancel each other except for the central peak (i.e., the desired image). Thus, the influence of the cavity effects on the image decreases gradually, and the field intensity distribution gradually transits to the simple shape for a LHM slab of infinite length. For a thicker slab, the resonance becomes weaker [see Fig. 3(b)], and its influence on the image quality decreases because of its evanescent characteristics along the z direction and the larger distance between the image plane and the bottom surface of the slab. It is also less sensitive to the length of the slab. In our simulation for $d = \lambda$ and $L > 7\lambda$, one can obtain a clear image with FWHM less than 0.3λ (along the image plane the intensity of these additional peaks are always less than 30% of that of the central peak, and the negative streams are less than 2%). Similarly, as we have verified numerically, the material loss of the LHM slab also damps the excitation of surface plasmons and the cavity effects.

In conclusion, the imaging system formed by a LHM slab of finite length has been analyzed through a FDTD method. The cavity effects of surface plasmons excited by the evanescent components of the incident field have been studied and used to explain the observed bright spots along the surfaces of the LHM slab and counterintuitive negative values of the normal component of the energy stream at the image side of the slab. It has been shown that both the length and the thickness of the LHM slab greatly influence the cavity effects of surface plasmons and, consequently, the image quality.

The partial support of National Natural Science Foundation of China (under a key project grant; Grant No. 90101024) is gratefully acknowledged.

*Corresponding author.

Email address: sailing@ieee.org

- [1] V. G. Veselago, *Sov. Phys. Usp.* **10**, 509 (1968).
- [2] R. A. Shelby *et al.*, *Science* **292**, 77 (2001).
- [3] J. B. Pendry, *Phys. Rev. Lett.* **85**, 3966 (2000).
- [4] D. R. Smith *et al.*, *Phys. Rev. Lett.* **85**, 2933 (2000); C. G. Parazzoli *et al.*, *ibid.* **90**, 107401 (2003); A. A. Houck *et al.*, *ibid.* **90**, 137401 (2003); J. Pacheco *et al.*, *ibid.* **89**, 257401 (2002); A. A. Zharov *et al.*, *ibid.* **91**, 037401 (2003).
- [5] N. Garcia *et al.*, *Phys. Rev. Lett.* **88**, 207403 (2002).
- [6] D. R. Smith *et al.*, *Appl. Phys. Lett.* **82**, 1506 (2003).
- [7] A. Taflov, *Computational Electrodynamics: The Finite-Difference Time-Domain Method* (Artech House, Boston, 1995).
- [8] S. A. Cummer, *Appl. Phys. Lett.* **82**, 1503 (2003).
- [9] R. Rupp, *J. Phys. Condens. Matter* **13**, 1811 (2001).